SPACE TELESCOPE SCIENCE INSTITUTE
Operated for NASA by AURA

Instrument Science Report WFC3 2007-03

Performance of the WFC3 Replacement IR Grisms

S. Baggett (STScI), R. Boucarut (GSFC), R. Telfer (OSC/GSFC),
J. Kim Quijano (STScI), M. Quijada (GSFC)
March 8, 2007

ABSTRACT

The WFC3 IR channel has two grisms, the G102, a relatively high-resolution "blue" element (800-1100 nm, R~200) and the G141, a relatively low-resolution "red" element (1100-1700 nm, R~140). This report summarizes the performance of the replacement G102 and G141 grisms installed in the WFC3 IR filter wheel in Nov 2006. The intent is to document the as-built properties and the characterization test results for the replacement grisms.

Introduction

WFC3 imaging during the first thermal vacuum (TV) ground test in the fall of 2004 revealed that while the IR filters performed as expected, well within specification, the IR grisms produced significantly out-of-focus (>2000 μ), slightly tilted spectra (Bushouse & Hartig 2005). The problems were traced to an error in the grism installation procedure - a 90 deg offset in the mounting of the grism due to the mislabeling of a coordinate system - and a slight rotation error (~8 deg) in the dispersion axes relative to the detector axes (Turner-Valle 2005). The cause of the latter issue was further resolved as an oversight in the alignment documentation, where it had been assumed that the filter wheel radius vector and the IR detector edge are parallel when they are in fact ~8 deg different.

Due to the orientation issues, the WFC3 team at GSFC and STScI, with WFC3 Scientific Oversight Committee (SOC) approval, decided to remove the grisms with the intention of re-installing them into the IR filter wheel with the correct alignment. Since the grisms

were being removed anyway and the master grating template was still available, the decision was taken to remake the G141 with a new red-side coating to reduce the somewhat higher-than-expected background seen in TV data due to the transmission of thermal background radiation. A new grism was procured and before it and the original G102 were installed into the IR filter wheel, lab tests were performed to verify the optical performance. The experiments were carried out using an optical setup (FilterGEISt) originally developed to simulate a WFC3-like beam for UVIS replacement filter characterizations and later modified to provide an IR channel-like beam (Telfer 2007a). Analysis of the test images showed that the grisms were considerably out of focus even when used in the correct orientation: ~230μ of defocus in G141 and ~500μ of defocus in G102. A re-examination of the TV data confirmed that the intrinsic defocus was indeed present but had been masked by the effects of the rotation error. Further investigation determined that the multi-layer bandpass coatings on the grism, the first step in the grism manufacturing process, were distorting the optic; the subsequent grating replication steps produced essentially a plano-convex lens which shortened the focal length. Optical modeling based on reflective interferometry (Hartig 2006) of the curved surface corroborated the lab results.

Figure 1: Schematic of the primary manufacturing steps and their effects on focus. The grism begins as a bare substrate with the intended focal length (top figure). The bandpass coatings, applied to one side of the element only, induce hoop stresses which distort the optic but the effect on focus is minimal since the result is effectively a meniscus lens (middle figure). After the resin is applied and the grating replicated, however, the element becomes a plano-convex lens, which shortens the focus (bottom figure).

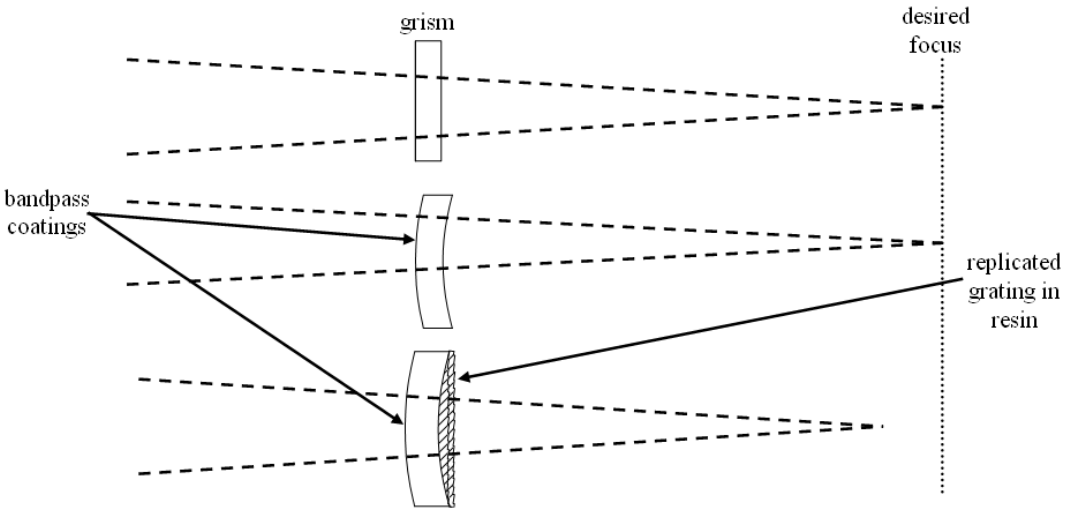

As the intrinsic defocus would render the grisms unusable on-orbit, thicker versions were procured to compensate for the focus shift; the rulings were reproduced, on new Hoya IR 80 color glass substrates, using the same master templates employed for the original grisms. The resulting grism candidates were tested extensively in the lab and the charac-

terization results evaluated in light of the requirements; the final choice of specific grisms to use as flight was determined by the SOC with input from the WFC3 team at GSFC and STScI (Baggett et al., 2007). The remainder of this report summarizes the characterization test results of the replacement grisms chosen for flight, documenting the as-built properties for future reference.

Characterization Results

The tests performed on the replacement grism candidates in the lab were based upon those used during validation of the original grisms and included inspections, verification of physical dimensions, and measurements of wavefront quality, throughput, and dispersion. Further tests were added to the suite in order to verify compliance with the CEI focus shift and ghost specification as well as environmental requirements. Individual lab reports detailing all test procedures and results for each grism are archived on the private Goddard Space Flight Center WWW site and are available upon request. Approval of the final flight grisms was provided by the WFC3 SOC, with input from the STScI and GSFC WFC3 team; the grisms selected for flight were #39 for G102 (G102-039) and #16 for G141 (G141-016).

Evaluation of the grisms made use of both spectral and imaging lab data. The spectral scans of witnesses were acquired using a Perkin Elmer spectrophotometer (PE 950); details of the scanning test setup and procedure have been documented in Quijada et al. (2006). Imaging data were acquired with FilterGEISt, a lab setup which can simulate the IR channel f/11 beam (Telfer 2007a). Images were collected with an InGaAs camera for the IR (900-1700 nm) and a CCD camera for the blue side of G102 (700-1100 nm). The cameras were rotated 24 deg to match the tilt of the WFC3 IR detector; the grisms were oriented to ensure the proper angle of incidence (listed in Table 1 below). Point source images for wavefront, focus, throughput, and dispersion measurements were taken in a 3x3 grid of 11 mm beams across the grism, completely covering the WFC3 IR full-field footprint on the grism. Sets of images at a range of focus settings were collected for wavefront and focus measurements while sets of images at a range of wavelengths were collected for dispersion and throughput measurements. In addition, white-light images were taken at a variety of rotation and translation positions in order to check for ghosts. The results from each of these tests will be discussed in more detail in the sections that follow.

Dimensions

For reference, some of the key grism design parameters are listed in Table 1. Dimensions of the elements are validated by the vendors (Barr Associates and Richardson Grating Labs) and confirmed upon receipt of the elements at GSFC. The prism apex angle was ver-

ified at GSFC using an auto-collimating theodolite with a calibrated precision rotary table; differences between the specification and the measurements were much less than 0.1deg, easily satisfying the 0.25 deg tolerance. As noted in the table, the new grisms were intentionally made thicker than the design called for, in order to compensate for focus. The final thicknesses (average of the thick and thin-side thicknesses) were measured as 3.950 and 4.064 mm for G102 and G141, respectively.

Table 1. Key grating design parameters, taken from GSFC IR Grism Specification document (Boucarut 2003).

requirement	G102	G141
blaze wavelength (μ)	1.01	1.34
prism apex angle (deg)	3.8557	2.82359
groove freq	58.0645	30.674
groove period (μ)	17.2222	32.6009
groove angle (deg)	6.00	4.267
angle of incidence (deg)	2.50058	1.83644
prism diameter (mm)	25.37	25.40
prism center thickness (mm)	3.135[a]	3.340[a]

a. These were the original design thicknesses; the new grisms are intentinally thicker than this in order to compensate for defocus (see text).

Throughput

The vendor provides witness pieces (substrates coated at the same time as the flight candidate elements) for spectral scanning; these are used to assess the quality of the bandpass coating before the resin is applied and the grating replicated on the coated flight candidate prisms. The color glass of the substrate (Hoya IR80) along with the longpass coating, must block the second-order diffraction wavelengths on the blue side while the short-pass coatings must provide blocking on the red side. Some iterations of the coating process were necessary, in order to obtain the desired bandpass edges, particularly the red side of the G141 grism which was to match the red edge of the F160W filter. Spectral scans of the witness pieces for the final replacement grisms are presented in Appendix A; a summary of the in- and out-of-band behavior is shown in the table below; wavelengths are air. For the out-of-band (OOB) information, the blue-side wavelength is the red limit of the OOB range shortward of the passband while the red-side wavelength is the blue limit of the OOB range longward of the passband.

Table 2. IR grism spectral parameters; requirements are in the first row; measurements, based upon the witness scans (shown in Appendix A), are in the second row. There was no OOB scan on the G141 witness.

grism	In band				Out of Band				type
	center wavelength (nm)	FWHM (nm)	blue edge (nm)	red edge (nm)	blue side, wavelength (nm)	blue side, max T	red side, wavelength (nm)	red side, max T	
g102	1025	250	900	1150	850	5×10^{-5}	1157	5×10^{-5}	spec
	965	360	786	1145	722	$<5 \times 10^{-5}$	1342	5×10^{-5}	meas
g141	1410	600	1080[a]	1700	917.7	5×10^{-5}	1690[b]	5×10^{-5}	spec
	1379	594	1082	1676	--	--	--	--	meas

a. Blue edge of G141 was initially specified as 1100 nm but later amended to 1080 nm in order to provide a larger overlap region with G102.

b. Set as “n/a” in the original specification document (no red coating was on the original grism), this was subsequently specified as 1690 nm, in order to reduce some of the background observed in TV due to thermal background radiation.

Of more relevance to potential users of the grisms are throughput curves for the completed elements (substrate + bandpass coating + replicated grating). The measurements were made from slightly defocused point source images taken via FilterGEISt; the data were taken with the grism in and out of the beam, covering the entire wavelength range in 10 nm steps (an IR camera was used in the 900-1750 nm range, while a CCD camera was used for the G102 blue side, 700-1100 nm). These throughput scans were performed at nine positions on the grism; data from each position were analysed separately. All images were first dark-corrected using a dark frame taken immediately following each target frame; aperture photometry was then used to measure the integrated fluxes, and the final throughput was computed as the ratio of the grism-in to grism-out fluxes.

The throughput results for the replacment grisms are shown in Figure 2; the curves from all nine positions were similar and have been averaged for each grism. The G102 throughput in the IR-CCD overlap region (900-1100 nm) were in good agreement and have been averaged in the plots shown. The results in Figure 2 include a small correction factor, ~1%, applied to the GSFC data; Appendix B describes the determination of this factor in more detail. Based upon the corrected curves, G141 easily meets the requirement of at least 80% peak efficiency, with a peak throughput of ~85%; the G102, with a ~79% peak, falls just below the requirement.

The new grism throughput curves have been incorporated into the STScI Synthetic Photometry (SYNPHOT) tables for use in the WFC3 calibration pipelines and in the web-based exposure time calculator (Brown 2006).

Figure 2: First-order throughput measured for the new flight G102 (left) and G141 (right); shown is the average of nine pointings across the grism. For G102, the CCD and IR camera results in the overlap region (900-1100 nm) were in good agreement and have been averaged as well.

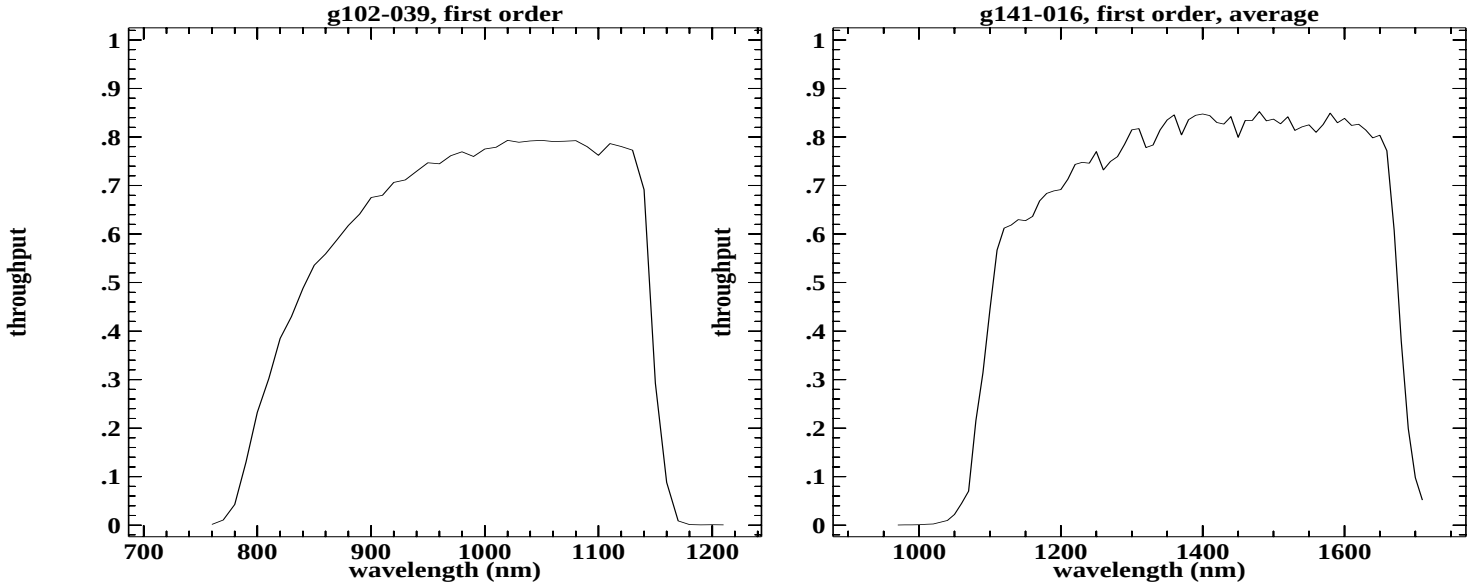

Dispersion

The linear dispersion was derived from nine in-focus wavelength sweeps taken at various locations across the grism, obtained with the FilterGEISt setup as described earlier in this report. The acquired images were dark-corrected and point source centroids measured. A linear fit to the target positions as a function of wavelength yielded the dispersion; the results quoted here have been converted from the InGaAs camera pixel scale to that of WFC3. Note that these measured dispersions are intended as a general check only; the exact dispersion of the new grisms, when used in WFC3, are expected to be slightly different from the measurements shown here depending upon the precise distance between grism and detector as well as the effects of the WFC3 IR camera window.

For G102, the average measured dispersion from the nine scans was 2.51 nm/pix (WFC3 pixels), with a standard deviation of 0.002 nm/pix; for comparison, the predicted dispersion for G102 in FilterGEISt is 2.52 nm/pix (the predicted dispersion in WFC3 is 2.47 nm/pix). For G141, the average measured dispersion was 4.67 nm/pix, with a standard deviation of 0.005 nm/pix; the predicted dispersion for G141 in FilterGEISt is 4.79 nm/pix (predicted dispersion in WFC3 is 4.69 nm/pix). The small differences between the model WFC3 and model FilterGEISt dispersions are due to a minor procedural error in the placement of the grism: in FilterGEISt, the grism was 123.5 mm from the focal surface while in WFC3, this distance is 127.5 mm (or 123.5 mm from the exit surface of a nominal filter).

The small differences between the measured and model values are attributed to unavoidable uncertainty in the placement of the grism relative to the detector.

To quantify the effect of distance between the grism and the detector on the resulting linear dispersion, wavelength sweeps were taken with a candidate G141 grism at a variety of relative grism/detector positions. Figure 3 shows the measured and model dispersions as a function of translation distance. Here, the dispersion is given in units of distance on the detector (in mm/nm) vs wavelength; positive translations correspond to smaller distances between grism and detector. As can be seen in the figure, the models show that moving the grism and moving the detector are equivalent (in FilterGEISt, the detector must be moved to change the grism/detector distance since the grism is not on a translatable stage). Also apparent is that while the models and measured data are slightly offset, attributed to small errors in positioning of the grism/detector pair, the slopes are nearly identical. The change in linear dispersion per unit translation, or slope, provides the angular dispersion which is independent of the grism/detector distance; the measured and model slopes agree to ~0.3%. Furthermore, the angular dispersion can be inverted to derive a groove period: the result is ~2% smaller than the G141 nominal value of 32.6, attributed to a small dispersive component inherent in the prism. The good agreement of the derived groove period to the nominal value is not unexpected, as the new grisms were produced using the same master ruling template employed to manufacture the original grisms.

Figure 3: Dispersion as a function of distance between detector and grism. Symbols represent the model and measured cases as noted in the legend; lines are the resulting linear fits.

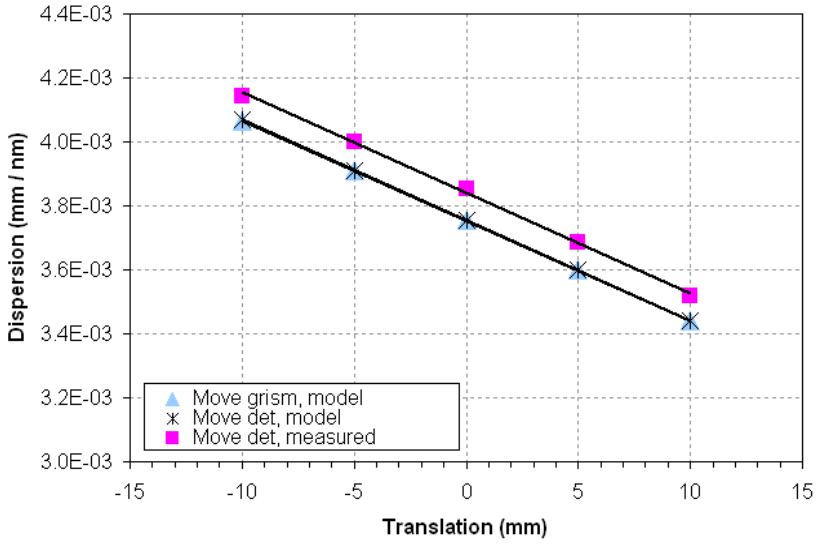

Focus

The specifications require the IR filter elements to be parfocal; that is, the elements must provide a focal shift equivalent to 4.0 mm +/- 0.1 mm of fused silica at 1000nm. Focal shifts for the grisms were measured from focus sweep data: a series of images of a point source taken at a variety of defocus levels; focus sweeps were obtained at each of nine positions arrayed in a 3x3 pattern across the grism. Reference focus sweeps (without the grism in the beam) were taken as well, and used to correct the grism scans. Phase retrieval analysis (point source fitting), including focus, yields the wavefront error and focus shift; details of the analysis procedure have been documented in Telfer (2007b).

The grism/detector separation investigations described in the dispersion section also revealed that the focus depends slightly on this distance because the grisms have optical power (an ideal grism would show no dependence as the focal shift occurs entirely inside the optic). The figure below presents the model focal shift dependence as a function of grism/detector distance, using reasonable surface curvatures for G141 and G102. A correction for the grism focus measurements was estimated using the translation errors derived from the linear dispersion measurements (including the 4 mm procedural error mentioned in the dispersion section). For the selected replacement grisms, the setup error was in the opposite sense of the procedural error, minimizing the magnitude of the correction (~0.01 mm or less). Table 3 summarizes the focus results.

Figure 4: Change in focus as a function of grism-detector separation. Results of the modelling are shown as symbols; lines are linear fits to the data.

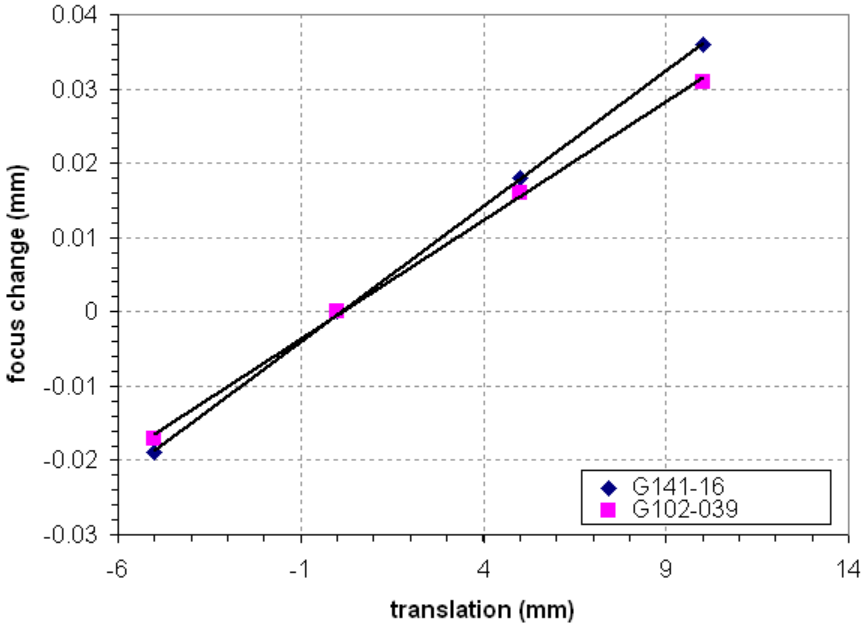

Quantities listed in Table 3

Avg focus shift: focus shift, in mm, the average of the nine pointings.
Measured focus error: difference, in mm, between the measured focus shift and the specification (1.2422 mm).
Translation error (total): sum of the procedural error (4.0 mm for both grisms) and a small setup error.
Distance: distance between the detector and the front of the grism (in mm).
Correction: correction applied to the measured focus to account for translation errors.
Final corrected focus error: measured focus error corrected for translation errors.

Table 3. Measured focus for replacement grisms.

quantity	g102-039	g141-016
average focus shift (mm)	1.224 +/- 0.034	1.2456 +/- 0.027
measured focus error (mm)	-0.019	0.003
translation, total error (mm)	2.9	1.0
distance: detector to front of grism (mm)	124.6	126.5
correction (mm)	-0.012	-0.004
final corrected focus error (mm)	*-0.030*	*0.000*

Wavefront

The transmitted wavefront error (WFE) over the 22 mm diameter clear aperture was originally required to be less than 0.02 waves at 633 nm in the CEI specifications. However, this specification could not be met by even ideal grisms, since their very design introduces some wavefront error. Furthermore, there is some field dependence because of focus, since the grism is thicker on one end. For this reason, the wavefront requirement has been revised for the grisms such that the total WFE should be less than the maximum design WFE added (linearly) to the 0.02 waves, computed for each of the 3x3 pointings individually. The expected WFE's for the IR grisms in the instrument as calculated with Zemax, at field center and central wavelength, were 0.094 for G102 and 0.050 for G141 (Telfer 2006); the measured field center WFE's were well under those values, at 0.0616 and 0.0365 for G102 and G141, respectively. The WFE of the other 8 pointings on each grism met the revised requirement as well (results for all pointings have been archived on the GSFC WWW site and are available upon request).

Ghosts

The CEI requirement calls for no more than 0.2% of the total light to fall within a discrete ghost. Both of the grisms satisfy this specification: ghosts are at the ~0.1% level or less. The images in Appendix C summarize the grism white-light images taken in the lab at the 16 IR field points; the frames have been mosaic'ed together into their relative positions in

the field of view. The individual images are not to scale: each of the 16 images has been made as large as possible in order to highlight any features. There are small ghosts occasionally visible near the upper right of the first-order; these have been confirmed as due to the lab setup, not the grism. The grism ghost, when visible, can be found between zeroth- and first-order.

Environment

The grisms were tested for compliance with the environmental requirements (storage, launch, and in-orbit); the specifications require the grisms to be able to survive relative humidity of up to 50% and a temperature range of +/-40 C. Testing was performed on a flight-like grism as well as a coated witness sample; these pieces were subjected to repeated temperature cycling, down to a minimum of -50 C. Detailed inspections of the elements were made before and after the cycling, using a high power microscope; no changes to the grism or witness were observed (He 2006). All parts of the grism remained intact.

Summary

Replacement IR grisms have been procured and installed in the WFC3 IR filter wheel in order to address the defocus issues found in the original elements. This report has presented the as-built properties and characterization test results of the new grisms. A summary of the key measurements are presented in Table 4, showing the measured defocus, dispersion, peak throughput, red and blue bandpass edges, and ghost levels.

Table 4. Summary of key measured characteristics.

grism	part num	defocus (μ)	dispersion (nm/WFC3pix)	1st order T (max, %)	throughput blue edge (nm)	throughput red edge (nm)	ghost (%)
g102	039	19	2.51	79	824	1147	<0.05
g141	016	3	4.67	85	1099	1678	<0.2

Acknowledgements

The grism vendors, Barr Associates and Newport Rochester (Richardson Grating Labs), are thanked for their efforts in producing the best possible replacement grisms for WFC3. Thanks are also due to the extended WFC3 team at GSFC, STScI, and Ball, for input and advice during the process of procurement, characterization, and installation.

References

Baggett, S., et al., “Science Recommendation for Replacement IR Grisms,” in prep., 2007.

Boucarut, R. “WFC3 Infrared Grism Specifications Document, Version D,” GSFC, 2003.

Brown, T., “Filter Throughputs for WFC3 SYNPHOT Support,” WFC3 Instrument Science Report WFC3-2006-03, Sep 2006.

Bushouse, H., and Hartig, G., “WFC3 Thermal Vacuum Testing: IR Grism Focus and Tilt Anomalies,” WFC3 Instrument Science Report WFC3-2005-06, Feb 2005.

Hartig, G., priv. comm, 2006.

He, Charles, priv. comm., 2006.

MacKenty, J., Contract End Item Specifications (CEI), STE-66, version May 31, 2002.

Quijada, Manuel, et al., “Images and spectral performance of WFC3 interference filters,” SPIE May 2006, 6265-109.

Telfer, R., internal memo, 2006.

Telfer, R., “The FilterGEISt Setup for WFC3 Filter and Grism Image Testing,” Orbital Sciences Corp. Technical Memo WFC3-577-RCT-011, Jan 2007a.

Telfer, R., “Analysis of FiterGEISt Data on WFC3 Candidate Filters and Grisms,” Orbital Sciences Corp. Technical Memo WFC3-577-RCT-012, Jan 2007b.

Turner-Valle, J., “WFC3 IR Grism Modeling and Rotations,” Ball Aerospace and Technologies Corp. Systems Engineering Report OPT-079, March 2005.

Appendix A. Spectral scans of grism witness pieces.

Figure 5: In-band and out-of-band (OOB) transmission scans for the grism witness pieces (there is no OOB scan for the G141 witness). Note that these represent the band-pass coating only, without the application of a grating. Details of the scanning test setup and procedure can be found in Quijada (2006)

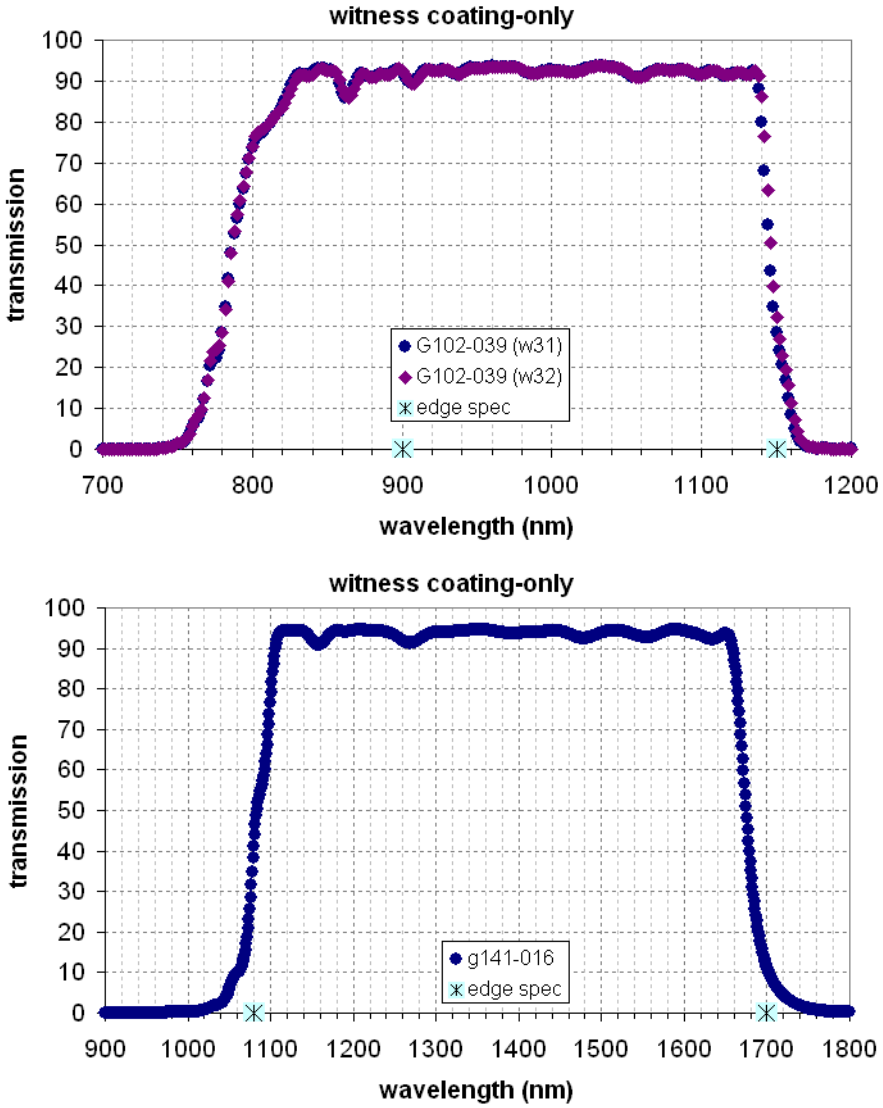

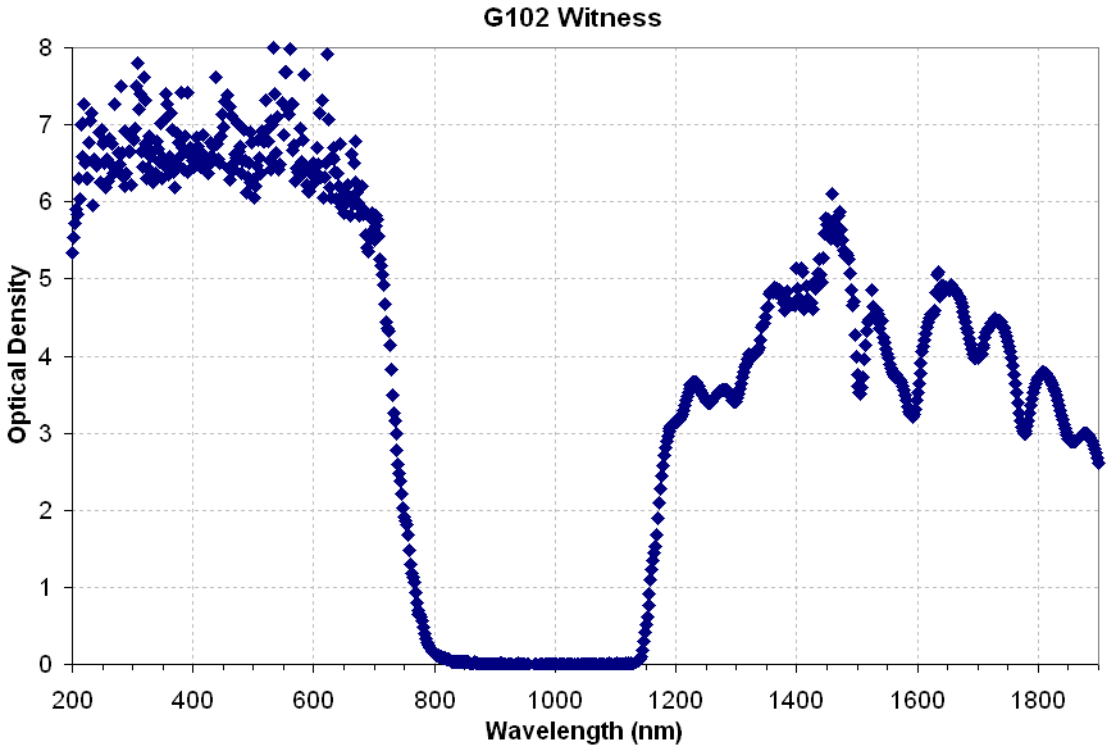
G102 Witness
Optical Density
Wavelength (nm)
0
1
2
3
4
5
6
7
8
200
400
600
800
1000
1200
1400
1600
1800

Appendix B. A small correction factor for the throughput results.

Richardson Grating Labs (RGL) provide a coarsely-sampled throughput curve with each grism delivery. Comparison of the throughput results from the FilterGEISt imaging and RGL revealed a small systematic offset: the RGL values were always slightly higher (by several percent) than those derived from the GSFC data. As mentioned in the Characterization section, the FilterGEISt measurement method consists of taking images with the grism in and out of the beam. The presence of the grism induces a slight focus shift relative to the grism-out configuration; any dependence of the measured flux on focus could cause a systematic effect in the throughput results. The FilterGEISt throughput images are also taken slightly out-of-focus in order to spread the point source light out on the detector. In the standard setup, the defocus is set to +5 mm; that is, the camera is moved 5 mm closer to the grism and the images without the grism are closer to focus than images with the grism.

To test the focus-effect hypothesis, the throughput of a G141 *witness* piece was measured in the standard way with FilterGEISt. The FilterGEISt setup was then modified to place the camera at the opposite focus setting (-5 mm), so that images with the grism were closer to focus than images without the grism, and the throughput was remeasured. Furthermore, since witness pieces do not have any resin or grating applied, a spectral scan of the optic's transmission was taken in order to provide a measure of the "true" throughput. The spectral scan was found to be systematically mid-way between the FilterGEISt throughput curves taken at +/- 5mm defocus. The throughput at the +5 mm (standard) defocus was on average about 1% lower than the level of the transmission scan across the entire wavelength range (~1100-1700 nm); the throughput at the -5 mm defocus was systematically higher than the transmission scan by a similar amount. Though the reason for the flux dependence on focus remains unknown, the FilterGEISt throughput results presented here have been corrected for this small factor. It should be noted that the correction was not enough to bring the GSFC and RGL measurements into complete agreement; the GSFC results remain systematically lower than the RGL values (by ~2% in G141 and ~3% in G102), attributed to differences in the two lab setups and/or measurement techniques. The final throughput of the grisms will be measured during upcoming instrument-level thermal-vacuum tests.

Appendix C. Mosaics of grism white-light images for G102 and G141.

Figure 6: Dispersion is in the +y direction: zeroth-order is the small point source at the bottom (or for G102, just off) each individual image; first-order is the larger source in the center/top. Small ghosts are occasionally visible near the upper right of the first-order; these have been confirmed as due to the lab setup, not the grism. The grism ghost, when visible, can be found between zeroth- and first-order, to the left of the center of the targets.